Journal of Magnetism and Magnetic Materials 569 (2023) 170444

Contents lists available at ScienceDirect

Journal of Magnetism and Magnetic Materials

journal homepage: www.elsevier.com/locate/jmmm

Computational modeling of hybrid micropolar nanofluid flow over a solid sphere

Hamzeh T. Alkasasbeh [a], Feras M Al Faqih [b], As'ad Alizadeh [c], Aissa abderrahmane [d,*], Mohammad Ali Fazilati [e], Hussein Zekri [f,g], Davood Toghraie [e,*], Abed Mourad [d], Kamel Guedri [h], Obai Younis [i,j]

[a] Department of Mathematics, Faculty of Science, Ajloun National University, P.O. Box 43, Ajloun 26810, Jordan
[b] Department of Mathematics, Al-Hussein Bin Talal University, Ma'an, Jordan
[c] Department of Civil Engineering , College of Engineering , Cihan University-Erbil, Erbil , Iraq
[d] Laboratoire de Physique Quantique de la Matière et Modélisation Mathématique (LPQ3M), University of Mascara, Algeria
[e] Department of Mechanical Engineering, Khomeinishahr Branch, Islamic Azad University, Khomeinishahr, Iran
[f] College of Engineering, The American University of Kurdistan, Duhok, Kurdistan Region-Iraq
[g] Department of Mechanical Engineering, College of Engineering, University of Zakho, Zakho, Kurdistan Region-Iraq
[h] Mechanical Engineering Department, College of Engineering and Islamic Architecture, Umm Al-Qura University, P.O. Box 5555, Makkah 21955, Saudi Arabia
[i] Department of mechanical engineering, college of engineering in Wadi Addwasir, Prince Sattam Bin Abdulaziz university, Al-kharj 11942, Saudi Arabia
[j] Department of Mechanical Engineering, Faculty of Engineering, University of Khartoum, Khartoum, Sudan

ARTICLE INFO

Keywords:
Solid Sphere
Mixed Convection
Hybrid nanofluid, MHD
Micropolar

ABSTRACT

The current study discusses the mixed convection boundary layer around an isothermal solid sphere utilizing numerical simulation; two fluid types of hybrid and mono micropolar nanofluids with constant wall temperature in an MHD field are examined. To improve a base fluid's thermophysical, optical, rheological, and morphological qualities, two different types of nanoparticles Copper oxide CuO and Graphite oxide (GO) are combined to create hybrid nanofluids. The sensitivity analysis was made to unveil the impacts of the mixed convection factor, the field strength and the micro-rotation factor. The results reveal that the improving effect of using NF by the induced micro-rotational effect is more prominent at lower angles and diminished at higher angles. Another point that could be obtained is that the thermal boundary layer thickness is directly proportional to the magnetic parameter; by increasing the M value from 0.5 to 2, the thermal boundary layer thickness increases from 1.4 to 1.8. Also, using hybrid instead of mono NF has nearly no effect on altering the angular velocity at $y > 4$; for other ones ($y < 4$), the difference is<15 %.

1. 1- introduction

It may be safe to say that in the last decade, nanotechnology has made great progress in many sciences, and for this reason, researchers have studied various a lot of aspects of this technology and the action of nanofluids, nanopowders, nanocomposites, nanochannels, etc [1–10]. Also, it is hard to imagine humans living in the current century without heat transfer. Most heat transfer processes in thermal systems are accomplished using heat transfer fluids (HTFs). The application of conventional HTFs (for example, water and ethylene glycol) is limited due to their low thermal conductivity [11]. To upgrade the energy efficiency of systems in engineering applications, conventional HTFs were replaced with nanofluids (NFs) [12]. NFs are suspension of small solid particles of metallic or non-metallic, called nanoparticles (NP), in the aforementioned base fluids [13]. With the higher thermal conductivity of NPs, the usage of NF improves heat transfer. Aydin and Guru [14] reviewed the NFs in terms of their preparation, stability, properties, and thermal performance. Although NFs are made by dispersing one type of NP in the base fluid, the thermal features of NFs could be boosted using hybrid NFs. Hybrid NFs are the mixture of two or more unlike NPs in the base fluid. Kamel et al. [15] presented the reviews the recent experimental studies focusing on the flow boiling heat transfer using nanofluids. The heat transfer due to permeable stretching tube in the presence of heat source/sink utilizing nanofluids studied by Ahmed et al. [16]. Ghachem et al. [17] discussed the magnetohydrodynamic natural

* Corresponding authors.
E-mail addresses: Toghraee@iaukhsh.ac.ir (D. Toghraie), ikmguedri@uqu.edu.sa, kmguedri@uqu.edu.sa (K. Guedri).

https://doi.org/10.1016/j.jmmm.2023.170444
Received 22 October 2022; Received in revised form 4 January 2023; Accepted 22 January 2023
Available online 25 January 2023

Nomenclature

C_p	Heat capacity $\left[J{\cdot}kg^{-1}{\cdot}K^{-1}\right]$
g	Acceleration due to gravity $\left[m{\cdot}s^{-2}\right]$
Gr	Grashof number
j	Micro-inertia density $\left[m^2\right]$
K	Micro-rotation parameter
k	Thermal conductivity $\left[W{\cdot}m^{-1}{\cdot}K^{-1}\right]$
$\overline{H}$	Angular velocity $\left[m{\cdot}s^{-1}\right]$
Pr	Prandtl number
T	The temperature of the fluid $[K]$
$\overline{u}$	$\overline{x}$-component of velocity $\left[m{\cdot}s^{-1}\right]$
$\overline{v}$	$\overline{y}$-component of velocity $\left[m{\cdot}s^{-1}\right]$

Greek Symbols

χ	Nanoparticles volume fraction
κ_0	Vortex viscosity $\left[kg{\cdot}m^{-1}{\cdot}s^{-1}\right]$
μ	Dynamic viscosity $\left[kg{\cdot}m^{-1}{\cdot}s^{-1}\right]$
ρ	Base fluid density $\left[kg{\cdot}m^{-3}\right]$
β	Thermal expansion coefficient $\left[K^{-1}\right]$
ϕ	Spin gradient viscosity $\left[kg{\cdot}m{\cdot}s^{-1}\right]$
ϖ	Stream function
θ	Dimensionless temperature

Subscripts

f	Base fluid
s	Solid particles
hnf	Hybrid nanofluids
w	Condition at wall
∞	Condition at infinity

convection in a cubical cavity equipped with a perforated separation. Ali et al. [18] presented the description of magnetohydrodynamic effects on the transient rotational flow of Oldroyd-B nanofluids. Appropriately NP types with specific weight percent are employed to achieve the desired heat exchange rate. Hybrid NFs found large applications in different aspects of human life [19,20,21]; in this way, the concept of hybrid NFs has been the subject of numerous numerical and experimental investigations. A comprehensive review on hybrid NF, their preparation methods, the influencing factors on their performance and their fields of application was presented by Salman et al. [22]. The water-based hybrid NF of Graphite and Silicon dioxide was prepared by Dalkılıç et al. [23], and its viscosity in various NP volumetric fractions and temperatures was measured. The viscosity increment by the volumetric fraction increase and temperature decrease was demonstrated; also, the greatest increase in viscosity was achieved. in the case of 2 % volume fraction and 15 degreesC temperature which was equal to 36.12 %. Hussein et al. [24] investigated numerically the mixed convection in a cubical cavity with active lateral walls and filled with graphene– platinum hybrid nanofluid. Recently, there have been studies about hybrid nanofluids near solid spheres and parallel plates, such as Patil et al. [25], Bhatt et al. [26] and Alkasasbeh [27]. The theory of rotating micro constituents effects in NFs firstly proposed by Eringen [28]. This Theory was introduced to cover the inability of the classical model to illustrate micro convection. Micropolar fluids have microstructures; in fact, these fluids contain random particles suspended in a viscous medium. The molecules in micropolar fluids have random translational and rotational motions. The micropolar NFs are classified as a new category of micropolar liquids; the presence of NPs in HTFs gives them a microstructure. Due to their numerous engineering applications, such as blood rheology, exotic lubricants, polymer extrusion and low-concentration suspension flows, the subject attracted numerous researchers for modeling the fluid flow, heat and mass transfer. Ariman et al. [29] reviewed the findings of Eringen [28] and different engineering applications of micropolar fluids explained by Lukaszewics [30]. Free convection of micropolar fluids in cavities has been explored by Aydin and Pop [31], Gibanov et al.[32] and Saleem et al.[33]. Hashemi et al. [34] researched the free convection of Cu/water micropolar NF in a porous medium containing a heat source. The Darcy model is used for modeling the flow dynamics, and the Galerkin finite element method is employed for solving the governing equations. Their results indicated that the Darcy number was in an inverse proportion with the fluid flow strength and micro-rotation of particles. Ahmed et al. [16] presented the laminar steady mixed convection flow field characteristics in a square lid-driven enclosure filled with water-based micropolar nanofluids numerically using the finite volume method. Hussanan et al. [35] investigated the transient free convection flow of five types of micropolar NF over a vertical plate. It was revealed that graphene oxide temperature suspended NF is higher than the other NFs. Izadi et al. [36] employed the thermal non-equilibrium model to examine the free convection flow of a micropolar NF in a porous cavity. It was demonstrated that by increasing the pores dimension and porosity, the governing equations could be converted to standard Navier–Stokes equations. Also, during rotation the NPs rotation, permeability affects the Nu number in the solid matrix. Abidi et al. [37] explored the fluid flow and heat and mass transfers (HMT) inside an enclosure filled with aqueous micropolar NF of Al_2O_3 subjected to a uniform magnetic field using a 3-D model. The sensitivity analysis was carried out to determine the influence of buoyancy ratio, Ra number, Ha number, NF concentration and micropolar material parameter on HMT and fluid flow. The authors also demonstrated that increasing the Ra and Ha numbers increased and decreased the heat and mass transfer rates, respectively. The implementation of magnetohydrodynamic (MHD) could improve heat transfer in many engineering applications. Alfven [38] introduced the concept of MHD fluid flow and described the MHD waves (Alfven waves). Rahbari et al. [39] performed an analytical and numerical study of the MHD flow in a parallel plate channel. The impact of the De, Ha, Re and Pr numbers on the velocity and temperature fields were investigated. It was shown that increasing the Ha number reduces the velocity values, whereas increasing the De number does not alter the velocity field significantly. Atif et al. [40] investigated the transient MHD squeezed flow having variable thermal conductivity with thermal radiation over the sensor surface. The nonlinear ordinary differential equations are implemented by the usage of the shooting technique. The sensitivity analysis was carried out to reveal the influence of the magnetic and Weissenberg number, squeezed flow index, power-law index, thermal radiation parameter and Pr number on velocity and temperature profiles. It was found that the permeable velocity, the Weissenberg number and the power-law index resulted in decreasing the velocity profile. Nazar et al. [41] studied the mixed convection boundary layer flow of a micropolar fluid around a sphere having a constant surface temperature. The Keller-box scheme was utilized for solving the non-similar boundary layer equations see [42]. It has been discovered that supporting flow retards boundary layer separation, and even at stronger flows suppress it. On the contrary, in opposing flow the separation point gets closer to the lower stagnation point and in case of strong flow the boundary layer would be eliminated. By the best of authors' knowledge. The available literature does not provide a significant contribution to the flow and heat transfer studies in themicropolar hybrid NF model. Considering the importance of MHD on improving the heat transfer rate it seems that the subject is of great value. Also, according to the literature review, the MHD stagnation

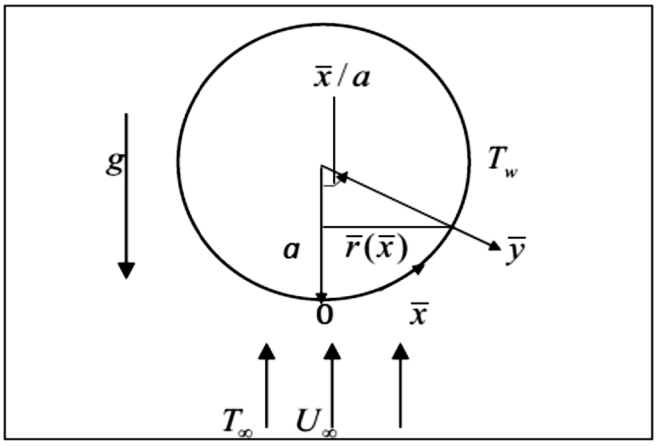

Fig. 1. Mixed convection physical model and coordinate system [33].

point micropolar NF flow with mixed convection has not yzet been examined. Here, the problem of mixed convection flow of water containing hybrid NP about a sphere within the MHD field is studied. In next section, the numerical approach is presented after presenting the problem and the governing equations. The results are discussed using the temperature profile, heat transfer coefficient, heat flux and friction factor diagrams and finally at last section the conclusion is presented.

2. The problem description and governing equations

As illustrated in Fig. 1, a mixed convection flow of water containing hybrid nanoparticles Copper oxide CuO and Graphite oxide (GO) about a sphere was assumed. The parameter × refers to the axis that is measured on the circumference of the sphere starting from the point of stagnation, while *y* refers to the axis that measures the perpendicular distance to its surface; q_w indicates constant heat flux, T_∞ the surrounding temperature of the liquid which is constant, and *g* stands for the gravity vector.

The continuity, momentum and energy equations for hybrid micropolar nanofluid are given by Eqs. (1) to (4), respectively[43–45].

$$\frac{\partial}{\partial \bar{x}}(\bar{r}\,\bar{u})+\frac{\partial}{\partial \bar{y}}(\bar{r}\,\bar{v})=0, \tag{1}$$

$$\bar{u}\frac{\partial \bar{u}}{\partial \bar{x}}+\bar{v}\frac{\partial \bar{u}}{\partial \bar{y}}=\bar{u}_e\frac{d\bar{u}_e}{d\bar{x}}+\left(\frac{\mu_{hnf}+\kappa}{\rho_{hnf}}\right)\frac{\partial^2\bar{u}}{\partial \bar{y}^2}+\frac{\beta_{hff}}{\rho_{hnf}}g(T-T_\infty)\sin\left(\frac{\bar{x}}{a}\right)+\frac{\kappa}{\rho_{hnf}}\frac{\partial \bar{H}}{\partial \bar{y}}-\frac{\sigma_{hnf}}{\rho_{hnf}}B_0^2\bar{u} \tag{2}$$

$$\rho_{hnf}j\left(\bar{u}\frac{\partial \bar{H}}{\partial \bar{x}}+\bar{v}\frac{\partial \bar{H}}{\partial \bar{y}}\right)=-\kappa\left(2\bar{H}+\frac{\partial \bar{u}}{\partial \bar{y}}\right)+\phi_{hnf}\frac{\partial^2\bar{H}}{\partial \bar{y}^2}, \tag{3}$$

$$\bar{u}\frac{\partial T}{\partial \bar{x}}+\bar{v}\frac{\partial T}{\partial \bar{y}}=\frac{k_{hnf}}{(\rho c_p)_{hff}}\frac{\partial^2 T}{\partial \bar{y}^2}, \tag{4}$$

The employed velocity and thermal boundary conditions over the sphere surface and the far way flow are according to Eqs. (5) and (6), respectively;

$\bar{u}=\bar{v}=0, T=T_w \bar{H}=-\frac{1}{2}\frac{\partial \bar{u}}{\partial \bar{y}}$ as $\bar{y}=0$, (5).

$\bar{u}\to\bar{u}_e(\bar{x}), T\to T_\infty H\to 0$ as $\bar{y}\to\infty$ (6).

In Eq. (5) $\bar{u}$ and $\bar{v}$ are the velocity components along the $\bar{x}$-$\bar{y}$ plane, respectively. The radial distance between the symmetrical axis and the sphere's surface is $\bar{r}(\bar{x})=a\sin(\bar{x}/a)$, and the local free-stream velocity is assumed $\bar{u}_e(\bar{x})=\frac{3}{2}U_\infty\sin\left(\frac{\bar{x}}{a}\right)$. The micro-inertia density and pin gradient viscosity of hybrid nanofluid are defined in Eqs. (7) and (8), respectively;

Table 1
The equations for determining the thermo-physical properties of hybrid NFs Alkasasbeh [27].

Coefficient of thermal expansion	$\beta_{hnf}=(1-\chi_2)\left[(1-\chi_1)\beta_f+\chi_1\beta_{s1}\right]+\chi_2\beta_{s2}$
Density	$\rho_{hnf}=(1-\chi_2)\left[(1-\chi_1)\rho_f+\chi_1\rho_{s1}\right]+\chi_2\rho_{s2}$
Viscosity	$\mu_{hnf}=\frac{\mu_f}{(1-\chi_1)^{2.5}(1-\chi_2)^{2.5}}$
Heat capacity	$(\rho c_p)_{hnf}=(1-\chi_2)\left[(1-\chi_1)(\rho c_p)_f+\chi_1(\rho c_p)_{s1}\right]+\chi_2(\rho c_p)_{s2}$
Thermal conductivity	$\frac{k_{hnf}}{k_{bf}}=\frac{(k_{s2}+2k_{bf})-2\chi_2(k_{bf}-k_{s2})}{(k_{s_2}+2k_{bf})+\chi_2(k_{bf}-k_{s2})}$, where $\frac{k_{bf}}{k_f}=\frac{(k_{s1}+2k_f)-2\chi_1(k_f-k_{s1})}{(k_{s_1}+2k_f)+\chi_1(k_f-k_{s1})}$
Electrical conductivity	$\frac{\sigma_{hnf}}{\sigma_f}=1+\frac{3\left[\frac{\chi_1\sigma_1+\chi_2\sigma_2}{\sigma_f}-(\chi_1+\chi_2)\right]}{\left[\frac{\chi_1\sigma_1+\chi_2\sigma_2}{\sigma_f}+2\right]-\left[\frac{\chi_1\sigma_1+\chi_2\sigma_2}{\sigma_f}-(\chi_1+\chi_2)\right]}$

Table 2
The non-dimensional forms of the employed parameters [27].

parameter	Dimensionless form
$\bar{x}$	$x=\frac{\bar{x}}{a}$,
$\bar{y}$	$y=\mathrm{Re}^{1/2}(\frac{\bar{y}}{a})$,
$\bar{r}(\bar{x})$	$r(x)=\frac{\bar{r}(\bar{x})}{a}$,
$\bar{u}$	$u=\frac{\bar{u}}{U_\infty}$,
$\bar{v}$	$v=\mathrm{Re}^{1/2}\left(\frac{\bar{v}}{U_\infty}\right)$,
$\bar{H}$	$H=\left(\frac{a}{U_\infty}\right)\mathrm{Re}^{1/2}\bar{H}$,
$\bar{u}_e(\bar{x})$	$u_e(x)=\frac{\bar{u}_e(\bar{x})}{U_\infty}$
T	$\theta=\frac{T-T_\infty}{T_w-T_\infty}$.

$$j=\frac{a\nu_f}{U_\infty} \tag{7}$$

$$\phi_{hnf}=\left(\mu_{hnf}+\kappa_0/2\right)j. \tag{8}$$

The values of coefficient of thermal expansion, density, viscosity, thermal diffusivity, heat capacity, thermal conductivity and electrical conductivity of hybrid NF, which are denoted by $\beta_{hnf}\rho_{hnf}\mu_{hnf}(\rho c_p)_{hnf}k_{hnf}$ and σ_{hnf}, respectively, are determined using their related equations as tabulated in Table 1.

To get the dimensionless form of the governing equations, some parameters are used; the dimensionless parameters are denoted without the bar sign over them and are shown in Table 2.

Inserting the previous variables into Eqs. (1) to (4), the dimensionless forms of boundary-layer equations are determined by Eqs. (9) to (12);

$$\frac{\partial}{\partial x}(ru)+\frac{\partial}{\partial y}(rv)=0, \tag{9}$$

$$u\frac{\partial u}{\partial x}+v\frac{\partial u}{\partial y}=u_e\frac{\partial u_e}{\partial x}+\frac{\rho_f}{\rho_{nf}}(D_1+K)\frac{\partial^2 u}{\partial y^2}+\frac{1}{\rho_{nf}}D_2\lambda\theta\sin x+\frac{\rho_f}{\rho_{nf}}K\frac{\partial H}{\partial y}-\frac{\rho_f}{\rho_{hff}}\frac{\sigma_{hff}}{\rho_f}Mu \tag{10}$$

Table 3
The non-dimensional parameters for the governing equations [27].

$D_1 = \frac{1}{(1-\chi_1)^{2.5}(1-\chi_2)^{2.5}}$	0
$D_2 = (1-\chi_2)\left[\chi_1\left(\rho_{s_1}\beta_{s1}/\beta_f\right)+(1-\chi_1)\rho_f\right]+\chi_2\left(\rho_{s_2}\beta_{s2}/\beta_f\right)$	0
$D_3 = \frac{k_{hff}/k_f}{(1-\chi_2)\left[(1-\chi_1)\rho_f+\chi_1(\rho c_p)_{s1}/(\rho c_p)_f\right]+\chi_2(\rho c_p)_{s2}/(\rho c_p)_f}$	0
$M = \frac{\sigma_f B_0^2 a^2 Gr^{-1/2}}{\rho_f \nu_f}$	the magnetic factor
$K = \kappa_0/\mu_f$	micro-rotation
$K = \kappa/\mu_f$	micro-rotation factor
$Pr = \nu_f/\alpha_f$	Prandtl number
$\lambda = Gr/\mathrm{Re}^2$	mixed convection parameter
$Gr = g\beta(T_w - T_\infty)a^3/\nu_f^2$	Grashof number

$$u\frac{\partial\theta}{\partial x}+v\frac{\partial\theta}{\partial y}=\frac{D_3}{Pr}\frac{\partial^2\theta}{\partial y^2} \tag{11}$$

$$u\frac{\partial H}{\partial x}+v\frac{\partial H}{\partial y}=-\frac{\rho_f}{\rho_{nf}}K\left(2\overline{H}+\frac{\partial\overline{u}}{\partial\overline{y}}\right)+\frac{\rho_f}{\rho_{nf}}\left(D_1+\frac{K}{2}\right)\frac{\partial^2 H}{\partial y^2} \tag{12}$$

In Eqs. (9) to (12) the non-dimensional quantities and their interpretations are shown in Table 3.

It is important to note that $\lambda > 0$ shows the case of an assisting flow ($T_w > T_\infty$) (heated flow), $\lambda < 0$ reveals the opposing flow ($T_w < T_\infty$) (cooled flow) and $\lambda = 0$ refers to the forced convection flow. Using the non-dimensional parameters, the boundary conditions (Eqs. (5) and (6)) get the form of Eqs. (13) and (14);

$u = v = 0, \theta = 1, H = -\frac{1}{2}\frac{\partial u}{\partial y}$ as $y = 0$(13).

$u \to u_e(x) = \frac{3}{2}\sin x u \to 0,\ \theta \to 0,\ H \to 0$ as$y \to \infty$. (14).

The following equations are assumed to solve Eqs. (9) to (12), subject to boundary conditions (Eqs. (13) to (14));

$$\begin{aligned}\psi &= xr(x)f(x.y),\\ H &= xh(x,y)\end{aligned} \tag{15}$$

Where ψ denotes the stream function that is related to × and y-velocity components according to Eqs. (16) and (17);

$$u = \frac{1}{r}\frac{\partial\psi}{\partial y} \tag{16}$$

$$v = -\frac{1}{r}\frac{\partial\psi}{\partial x} \tag{17}$$

The stream function ψ is defined in such a way that satisfies the continuity equation (Eq. (9)). By substituting Eq. (15) into Eqs. (9) to (12), the following transformed equations are obtained;

$$\frac{\rho_f}{\rho_{nf}}(D_1+K)\frac{\partial^3 f}{\partial y^3}+(1+x\cot x)f\frac{\partial^2 f}{\partial y^2}-\left(\frac{\partial f}{\partial y}\right)^2+\frac{D_2}{\rho_{hnf}}\lambda\frac{\sin x}{x}\theta+\frac{9}{4}\frac{\sin x\cos x}{x}+\frac{\rho_f}{\rho_{hnf}}K\frac{\partial h}{\partial y}-\frac{\rho_f}{\rho_{hnf}}\frac{\sigma_{hnf}}{\rho_f}\mathrm{M}\frac{\partial f}{\partial y}=x\left(\frac{\partial f}{\partial y}\frac{\partial^2 f}{\partial x\partial y}-\frac{\partial f}{\partial x}\frac{\partial^2 f}{\partial y^2}\right), \tag{18}$$

$$\frac{D_3}{Pr}\frac{\partial^2\theta}{\partial y^2}+f\frac{\partial\theta}{\partial y}(1+x\cot x)=x\left(\frac{\partial f}{\partial y}\frac{\partial\theta}{\partial x}-\frac{\partial f}{\partial x}\frac{\partial\theta}{\partial y}\right) \tag{19}$$

$$\frac{\rho_f}{\rho_{hnf}}\left(D_1+\frac{K}{2}\right)\frac{\partial^2 h}{\partial y^2}+(1+x\cot x)f\frac{\partial h}{\partial y}-\frac{\partial f}{\partial y}h-\frac{\rho_f}{\rho_{hnf}}K\left(2h+\frac{\partial^2 f}{\partial y^2}\right)=x\left(\frac{\partial f}{\partial y}\frac{\partial h}{\partial x}-\frac{\partial f}{\partial x}\frac{\partial h}{\partial y}\right). \tag{20}$$

The boundary conditions in transformed space would become as Eqs. (21) and (22);

$f = \frac{\partial f}{\partial y} = 0, \theta = 1 h = -\frac{1}{2}\frac{\partial^2 f}{\partial y^2}$ as$y = 0$, (21).

$\frac{\partial f}{\partial y} \to \frac{3}{2}\sin x\theta \to 0 h \to 0$ as$y \to \infty$. (22).

At the lower stagnation point of the sphere, i.e.$x \approx 0$, Eqs. (18) to (20) are reduced to the differential equations below:

$$\frac{\rho_f}{\rho_{nf}}(D_1+K)f''' + 2ff'' - (f')^2 + \frac{D_2}{\rho_{hnf}}\lambda\theta + \frac{\rho_f}{\rho_{hnf}}K\frac{\partial h}{\partial y} + \frac{9}{4} = 0, \tag{23}$$

$$\frac{D_3}{Pr}\theta'' + 2f\theta' = 0, \tag{24}$$

$$\frac{\rho_f}{\rho_{nf}}\left(D_1+\frac{K}{2}\right)h'' + 2f h' - f' h - \frac{\rho_f}{\rho_{nf}}K(2h+f'') = 0, \tag{25}$$

And the boundary conditions (Eqs. (21) and (22)) become Eqs. (26) and (27);

$$f(0) = f'(0) = 0,\ \theta(0) = 1,\ h(0) = -\frac{1}{2}f''(0) \text{ as } y = 0 \tag{26}$$

$$f' \to \frac{3}{2},\ \theta \to 0,\ h \to 0 \text{ as } y \to \infty, \tag{27}$$

Where the primes denote differentiation for y.

The physical quantities of concern are the C_f and Nu numbers, which may be represented as

$$Cf = \frac{a}{\mu_f U_\infty}\mathrm{Re}^{-1/2}\left(\left(\mu_{hnf}+\kappa\right)\frac{\partial\overline{u}}{\partial\overline{y}}+\kappa\overline{H}\right)_{\overline{y}=0} \tag{28}$$

$$\mathrm{Nu} = -\frac{k_{hnf}\,a}{k_f(T_w - T_\infty)}\mathrm{Re}^{-1/2}\left(\frac{\partial T}{\partial\overline{y}}\right)_{\overline{y}=0} \tag{29}$$

By calling the dimensionless variables in Table 3 and the boundary conditions (Eqs. (13) and (14)), the local skin friction factor Cf and Nu numbers could be written as Eqs. (30) and (31), respectively;

$$Cf = \mathrm{Re}^{-1/2}\left(D_1+\frac{K}{2}\right)x\frac{\partial^2 f}{\partial y^2}(x,0), \tag{30}$$

$$\mathrm{Nu} = -\mathrm{Re}^{1/2}\frac{k_{hnf}}{k_f}\frac{\partial\theta}{\partial y}(x,0). \tag{31}$$

3. The numerical method and validation

Eqs. (18)-(20) with their corresponding boundary conditions (Eqs. (21)-(22)) have been numerically solved utilizing the Keller-box approach once the proper value of y has been established, as explained in [34]. In this method, the numerical solution is obtained by considering the step size of 0.02 with a six-decimal places criterion of convergence for accuracy. In fact, one needs to consider the following four basic procedures in using the method:

i. Re-written the transformed Eqs. (18)- (20) with their corresponding boundary conditions (21)-(22) into a first order system of equations.
ii. Using the central difference method to convert the obtained first order equations into set finite difference equations.
iii. Newton quasi-linearization method is then employed in solving the system of non-linear equations.
iv. Block-matrix algorithm is finally used to solve the differential equations.

The velocity, angular velocity, and temperature distribution profiles are presented by adjusting controlling factors to obtain the physics of the problem. The controlling factors contain the mixed convection factor $-1 \le \lambda \le 1$, the micro-rotation factor$0.5 \le K \le 4$, and the mag-

Table 4
Thermophysical characteristics of the used base fluid and nanoparticles [27].

Property	H_2O	CuO	GO
ρ (kg/m^3)	997.1	6510	1800
C_p (J/kg/K)	4179	540	717
k (W/m/K)	0.631	18	5000
$\beta \times 10^{-5}(K^{-1})$	21	0.85	28.4
$\sigma(S/m)$	5.5 $\times 10^{-7}$	5.96 $\times 10^{7}$	6.30 $\times 10^{7}$
Pr	6.2	–	–

Table 5
Comparison of local skin friction factor with Newtonian fluid ($K = 0$), and M = 0, at Pr = 7 [33].

	$\lambda = -2$		$\lambda = 2$	
x	Nazar et al. [23]	Present	Nazar et al. [23]	Current study
0°	0.0000	0.000000	0.0000	0.000000
10°	0.3309	0.330911	0.4955	0.495455
20°	0.6304	0.630391	0.9605	0.960512
30°	0.8700	0.870049	1.3675	1.367475
40°	1.0242	1.024165	1.6931	1.693320
50°	1.0713	1.071311	1.9194	1.919401
60°	0.9922	0.992201	2.0350	2.034991
70°	0.7635	0.763520	2.0363	2.036345
80°	_	_	1.9273	1.927412
90°	_	_	1.7195	1.719501
100°	_	_	1.4313	1.431285
110°	_	_	1.0870	1.086981
120°	_	_	0.7152	0.715178

netic factor $0.5 \leq M \leq 2$ for both the assisting ($\lambda > 0$) and opposing ($\lambda < 0$) flows. The numerical solution begins at the lower stagnation point of the sphere, $x \approx 0$, using initial profiles provided by Eqs. (18) to (21) and proceeds around the circumference of the solid sphere to the separation point. The current results are only valid up to $\times = 120$ degrees. Table 4 illustrates the thermophysical characteristics of the base fluid water and nanoparticles namely Copper oxide CuO and Graphite oxide (GO), which are size small particle that ranges between 1 and 100 nm. To verify the present numerical approach, the values of local skin friction are compared against Ref. [33] for the regular Newtonian fluid with $K = 0, (\chi_1 = \chi_2 = 0)$, and M = 0, at Pr = 7 for, $\lambda = \pm 2$ as presented in Table 5. It is found that the current results are very consistent with previously published results, therefore validating the accuracy of the current model.

4. Results and discussion

The fluid flow and heat transfer characteristics are specified mainly using the Nu number and friction factor. In this section, the heat transfer and fluid flow over the sphere are investigated firstly by presenting the variation of Nu and *Cf* numbers; then, the fluid flow and thermal fields are inspected by presenting the temperature and velocity profiles in the next subsection.

4.1. Fluid flow and thermal performance analysis

4.1.1. The effect of magnetic parameter

The variation of the local Nu number vs the *x*-degree for magnetic parameters of 0.5, 1 and 2 is shown in Fig. 2. As shown, the Nu number is decreased by proceeding the way from the stagnation point toward the separation point; in the case of employing no MHD field (M = 0), the Nu number decreased from 2.2 to 0.4 W/m^2.K and from 1.8 to 0.5 W/m^2.K for hybrid and mono NFs which corresponds to reductions of 82 % and 72 %, respectively. The greater reduction of Nu number by the x-degree increment in the case of a hybrid than mono NF could be attributed to the higher enhancing effect of turbulence and reverse flow in mono NFs; this leads eventually to a higher Nu number of mono NF than hybrid NF at $\times = 120$. In the first values of $\times$, the Nu number is greater in the case of a hybrid rather than mono NF; at $\times = 0$ and M = 0, the local Nu numbers are 2.2 and 1.8 W/m^2.K for hybrid and mono NFs, respectively. The higher value of the Nu number for hybrid NFs rather than monotype is related to its higher thermal conductivity. The difference between the Nu number of mono and hybrid NFs is more pronounced in lower values of $\times$ and becomes less through the way from the stagnation point ($x = 0$); the trend becomes reverse at higher $\times$ values where the Nu number of mono is higher than hybrid NF. At M = 0 and $\times = 120$, the local Nu number is 0.4 and 0.5 W/m^2.K for hybrid and mono NFs, respectively. The point where the Nu number for hybrid and mono NFs are equal is not the same for different M numbers, and by increasing M, it is decreased.

The variation of friction factor vs the *x*-degree for mono and hybrid NFs and different M values is depicted in Fig. 3. As seen, the *Cf* is increased by passing from the stagnation point toward a specific point

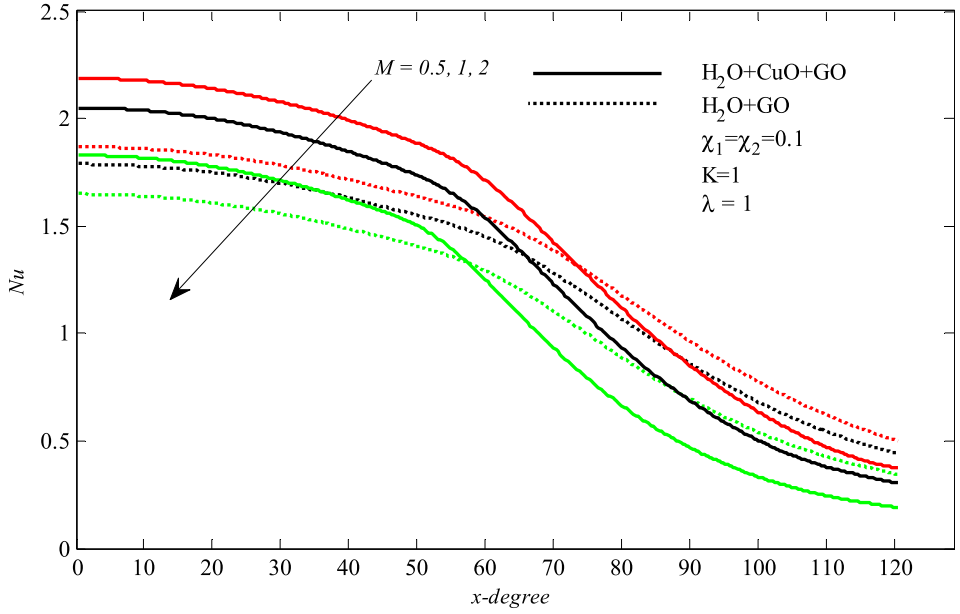

Fig. 2. Impact of magnetic parameter M on the local Nu number.

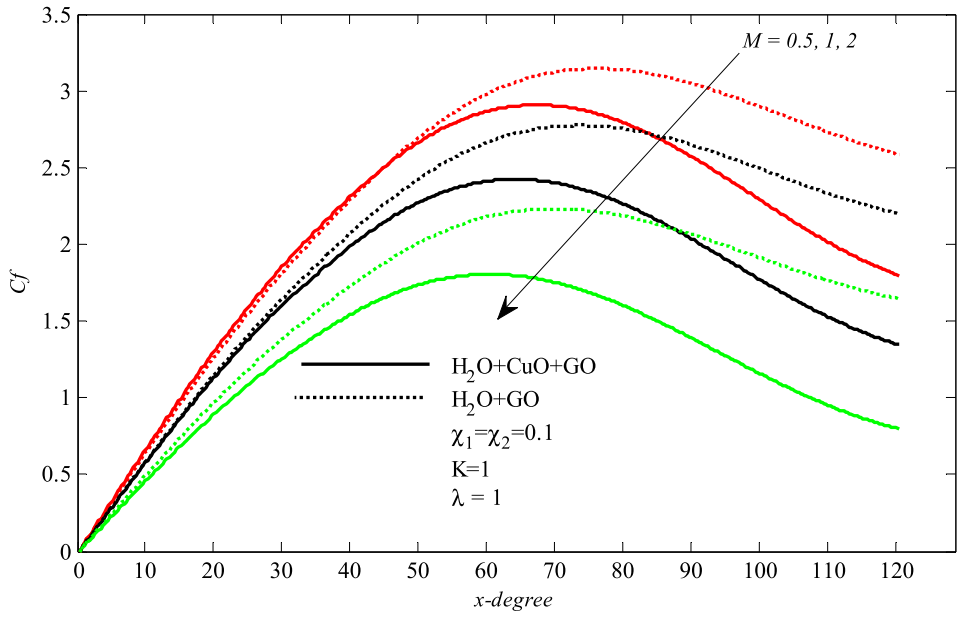

Fig. 3. Impact of magnetic parameter M on the local friction factor.

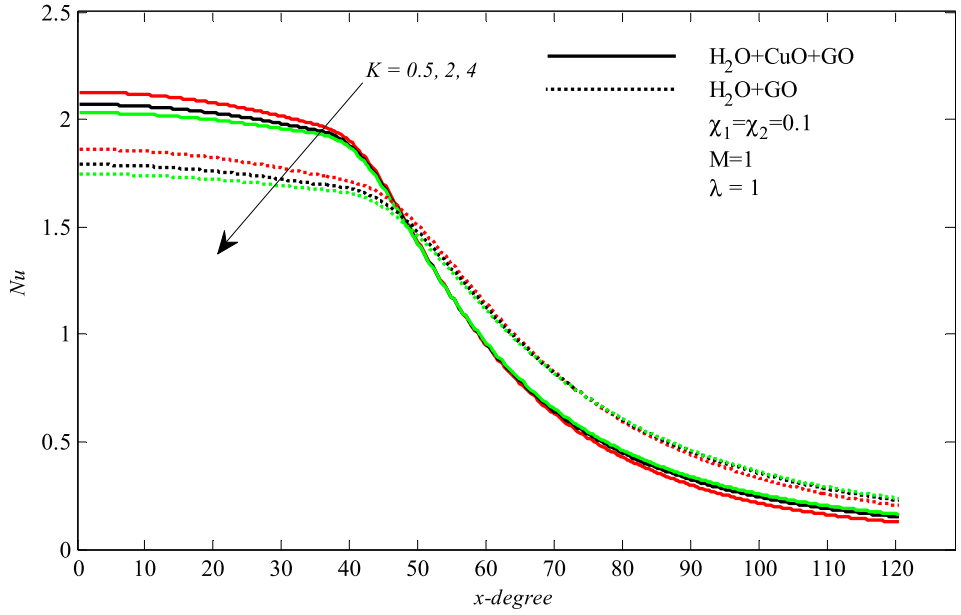

Fig. 4. Impact of micro rotation parameters *K* on the local Nu number.

and then decreasing. This trend which is repeated for all NF types and M numbers, is due to the presence of wakes and their growth by passing over the sphere. Also, by using hybrid instead of mono NF, the friction factor would be reduced. The present reduction of *Cf* by using hybrid in place of mono NF is more pronounced at higher values of *x*-degree; at M = 0 and at a location of 120 degrees, *Cf* is decreased from 2.6 to 1.75, which are equal at × = 0.

4.1.2. The impact of micro rotation parameter

To reveal the influence of the NF micro rotation factor on heat transfer rate, the variation of Nu number vs the location for M = 1 and different K values is depicted in Fig. 4. Similar to previous figures, the Nu number is decreased by passing from the stagnation point forward. In addition, in the first part of the fluid way and before the location of 50 degrees, the Nu number is greater in the case of using hybrid NF and afterward, the reverse is true. Another feature that may be deduced from the figures is that by increasing the parameter of micro-rotation, the Nu number would be increased in each case. This result reveals the improved effect of using NF by the induced micro-rotational effect is more prominent at lower angles and diminished at higher angles. This could be attributed to the creation and growth of the wakes by passing the fluid over the sphere's surface.

The variation of local friction factor vs the angular location for micro-rotation parameters of 0.5, 2 and 4 are depicted in Fig. 5. Increasing the micro-rotation parameter has an unfavourable effect on Cf and increases it; in the angular location of 120 degrees and for hybrid NF, by increasing K from 0.5 to 4, Cf is increased from 0.8 to 4.5. Also, in each case, Cf is higher in the case of using hybrid instead of mono NF by increasing their difference in higher angular positions. The increasing difference between the Nu number bypassing the NF over the sphere surface.

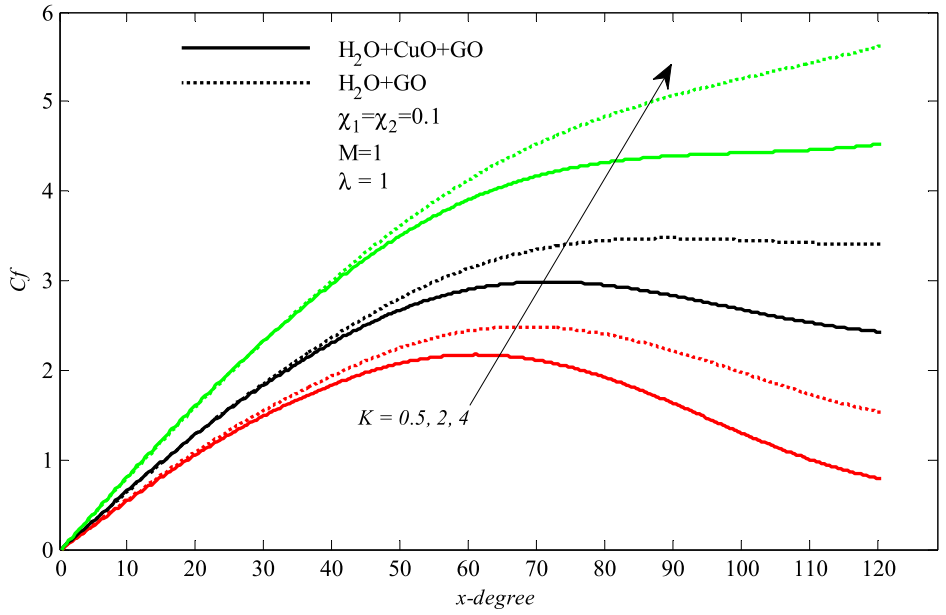

Fig. 5. Impact of micro rotation parameter K on the local friction factor.

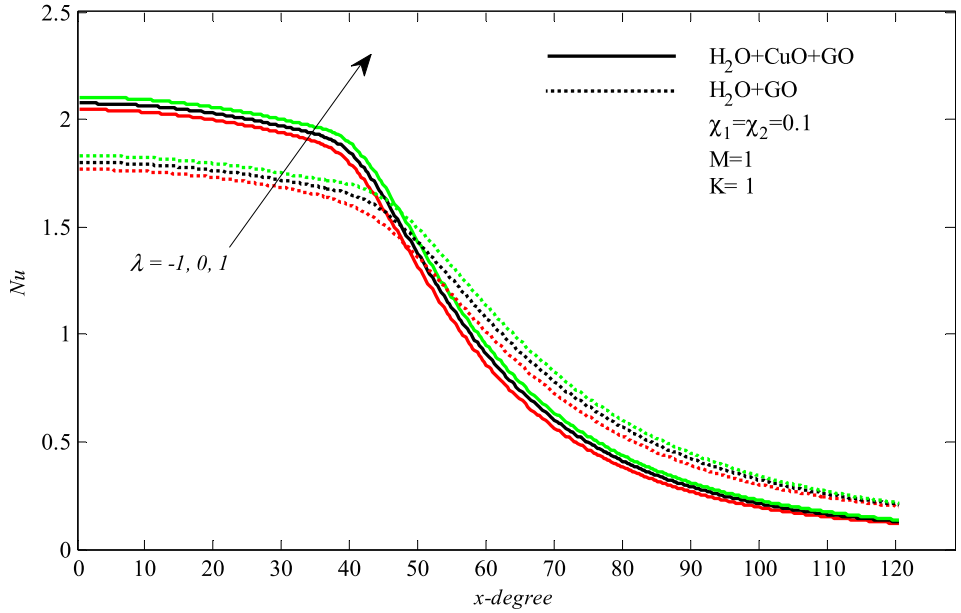

Fig. 6. Impact of mixed convection parameter λ on the. local Nu number.

4.1.3. The impact of mixed convection parameter

To examine the impact of mixed convection parameters on heat transfer, the variation of Nu number along the sphere surface for various values of λ is illustrated in Fig. 6. The mixed convection parameter specifies the heat transfer direction; $\lambda > 0$ denotes the heated surface $(T_w > T_\infty)$,$\lambda < 0$ is for the cooled sphere $(T_w < T_\infty)$. For small values of $|\lambda|$, the forced convection is dominated, whereas, for the larger values of $|\lambda|$, the natural convection is more important; for $|\lambda|$ values in order of 1 (which is the case here), both effects are comparable, and there is the mixed convection. By inspecting Fig. 6, it could be seen that the overall variation of Nu along the surface is decreasing for both types of NF. By moving along the surface from θ = 0 to 120 degrees, the Nu number changes from 2.1 to 0.2 and 1.75 to 0.25 W/m^2.K in the case of using hybrid and mono NF, which corresponds to reductions of 99 % and 98 %, respectively. This could be explained by the boundary layer's growing thickness which would alleviate the heat transfer coefficient at higher angles. The sensitivity of the Nu number from the variation of λ is very small and diminishes totally at higher x-degrees. The slight increase of the Nu number by increasing the value ofλ at high values of x-degree.

By inspecting the variation of friction factor along the sphere surface, as shown in Fig. 7, an increasing trend could be seen. This variation which is due to the formation of the vortex behind the sphere surface, is repeated in all cases of λs, but the value of Cf is higher in cases of greater values of λ. The higher friction factor in cases with higher λ *is* the result of surface condition; for $\lambda < 0$, the adjacent flow near the sphere is colder than the bulk fluid and therefore has higher local viscosity and vice versa, for $\lambda > 0$, the fluid is warmer and in this case the viscosity and the resulted Cf are both lower.

Another point that could be inferred from Fig. 7 is that the friction factor is lower in the case of using hybrid instead of mono NF. The

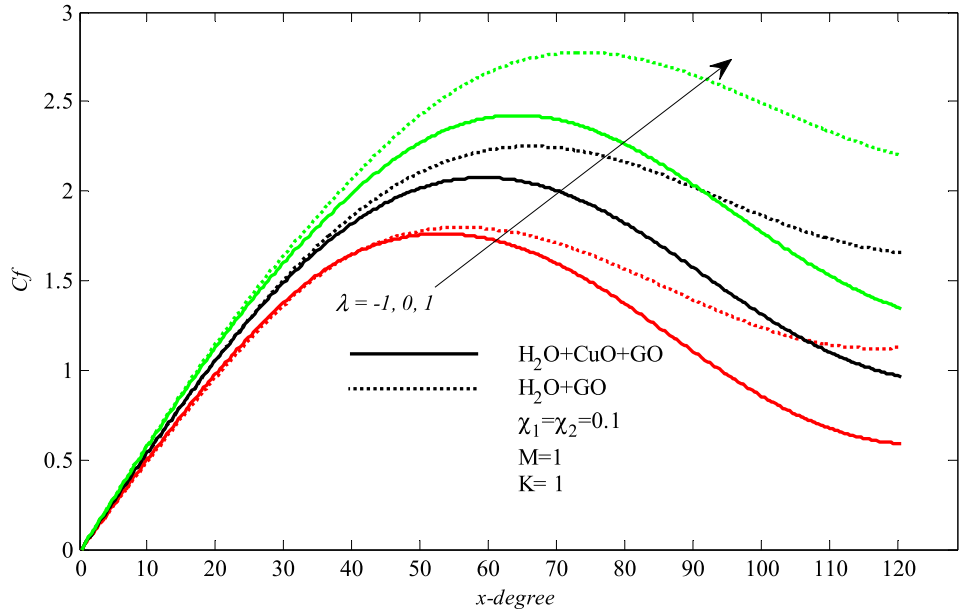

Fig. 7. Impact of mixed convection parameter λ on the local skin friction.

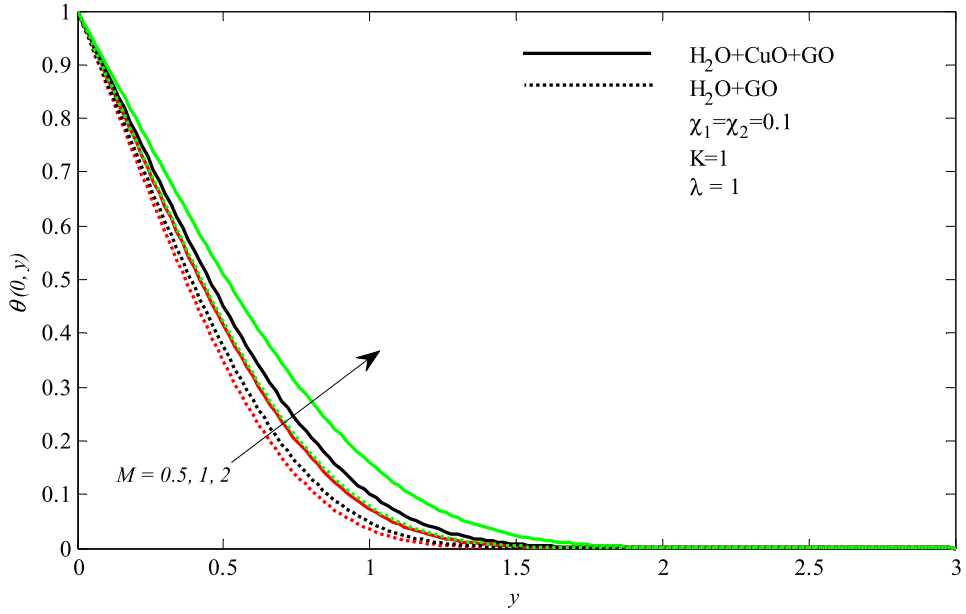

Fig. 8. Impact of magnetic parameter M on the temperature profiles.

difference between the *Cf* of hybrid and mono NFs is seen at all positions but is increased by increasing the value of the mixed convection factor; at an angle of 10 degrees, the difference between the *Cf* values in the case of using hybrid and mono NFs are 0.5, 0.7 and 0.9 for mixed convection parameters of −1, 1 and 0, respectively. This result shows that the higher reducing effect of using hybrid NF is in cases of high mixed convection parameters in which the sphere is cooling.

4.2. Fluid flow and thermal physics

To visualize the fluid flow and thermal fields, the temperature, velocity and angular velocity profiles for various values of magnetic, micro rotation and mixed convection parameters in cases of using mono and hybrid NFs are depicted in Fig. 8 to Fig. 16. The influence of altering M, *K* and λ on different evaluating parameters is depicted in Fig. 8 to Fig. 10, Fig. 11 to Fig. 13 and Fig. 14 to Fig. 16, respectively.

4.2.1. The impact of magnetic factor

The variation of dimensionless temperature (θ) at $\times = 0$ vs the *y* for magnetic parameters of 0.5, 1 and 2 and in cases of using mono and hybrid NFs is depicted in Fig. 8. As expected, the overall variations of θ are decreasing, which means that by going away from the sphere, the temperature is approaching free stream temperature. Although the temperature would ultimately reach the infinite temperature, using hybrid instead of mono NF delays this; for the magnetic parameter of M = 2, the thermal boundary layer thickness (as defined where $\theta = 0.01$) in cases of using mono and hybrid NF is 1.4 and 1.8, respectively. Another point that could be seen in Fig. 8 is that by increasing the magnetic parameter, the thermal boundary layer thickness is increased; by increasing the M value from 0.5 to 2, the thermal boundary layer

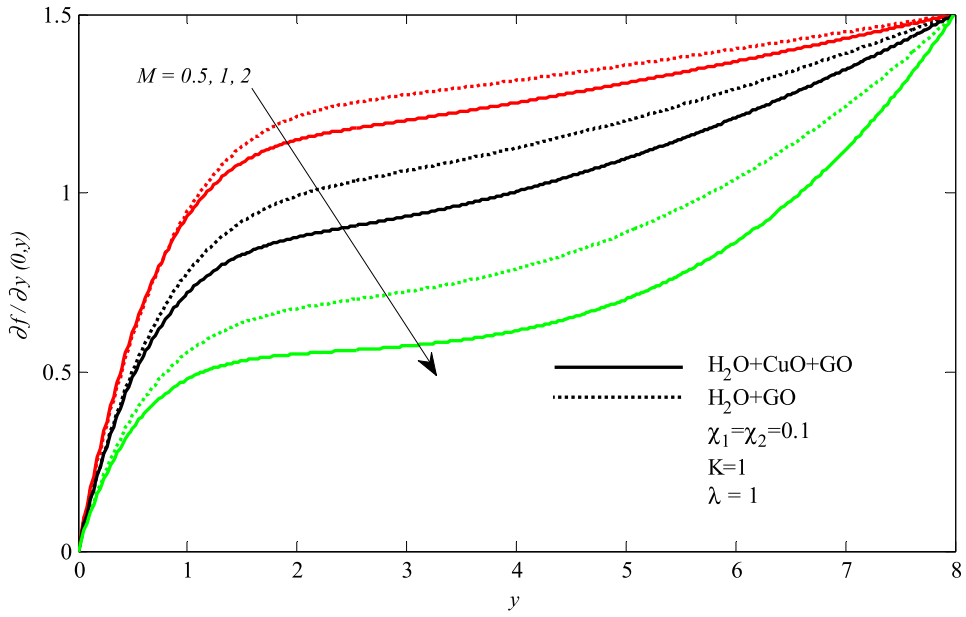

Fig. 9. Impact of magnetic parameter M on the velocity profiles.

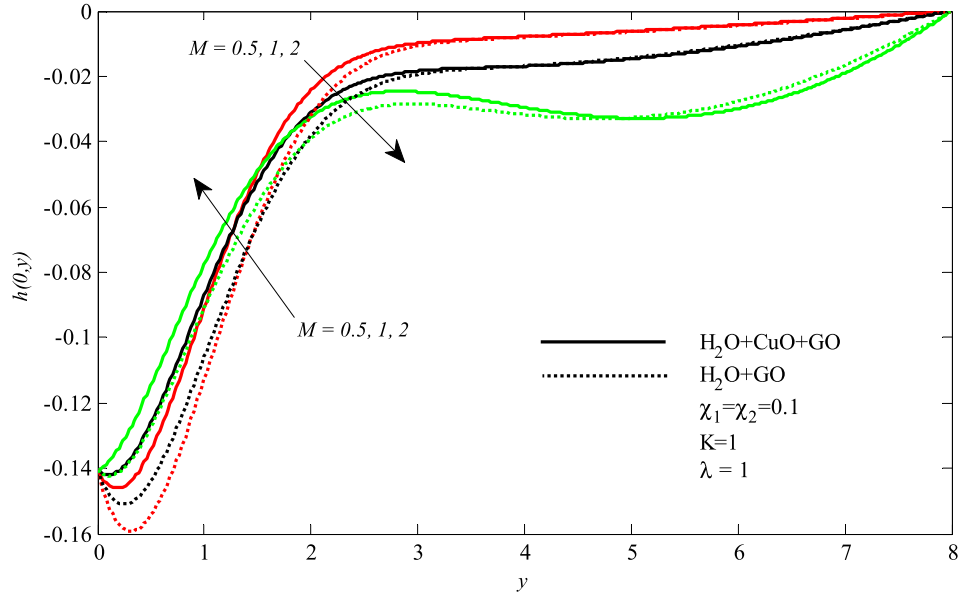

Fig. 10. Impact of magnetic parameter M on the angular velocity profiles.

thickness increases from 1.4 to 1.8.

Fig. 9 depicts the velocity profile along with the normal distance to the surface of the sphere in different magnetic parameters and $\lambda = 1$ (forced convection). As seen, the velocity changes from the value of zero at $y = 0$ to its maximum value at $y = 8$. Although at first (adjacent to sphere surface) and last points (far from the sphere surface) for all the study cases, the velocity is zero, but through the way \the fluid velocity differs; at each y, the fluid velocity is higher in case of mono rather than hybrid NF. For example, at M = 2 and y = 4, the non-dimensional velocity is 0.6 and 0.75 for hybrid and mono NFs, respectively. The higher value of fluid velocity in the case of using mono rather than hybrid NF. In addition, the higher velocity difference between the mono and hybrid at higher M numbers occurs because crossing a magnetic field through a moving fluid generates a force called the Lorentz force, which, as a result, boosts the resistance of the hybrid NF.

The variation of angular velocity vs the perpendicular distance from the sphere surface (y) at the stagnation point ($x = 0$) is shown in Fig. 10. Similar to the variation of velocity (Fig. 9), the angular velocity would be zero adjacent to the sphere surface and far from it but unlike velocity, the sensitivity of angular velocity to the magnetic number and fluid type (mono or hybrid NF) is less. Using hybrid instead of mono NF has nearly no effect on altering the angular velocity at y values>4, and for other ones ($y < 4$), the difference is<15 %. Unlike the fluid type, the magnetic number (M) has more effect in altering the value of angular velocity and is more prominent in $y = 5$ for M change from 0.5 to 2 and in $y = 3$ for M change from 1 to 2; by changing M from 0.5 to 2 the angular velocity changes about 57 % (from −0.35 to −0.15).

4.2.2. *The effect of micro-rotation parameter*

The effect of changing the micro-rotation parameter on the magnitude of the non-dimensional temperature profile in different y-positions from the stagnation point is shown in Fig. 11. As can be seen, for all

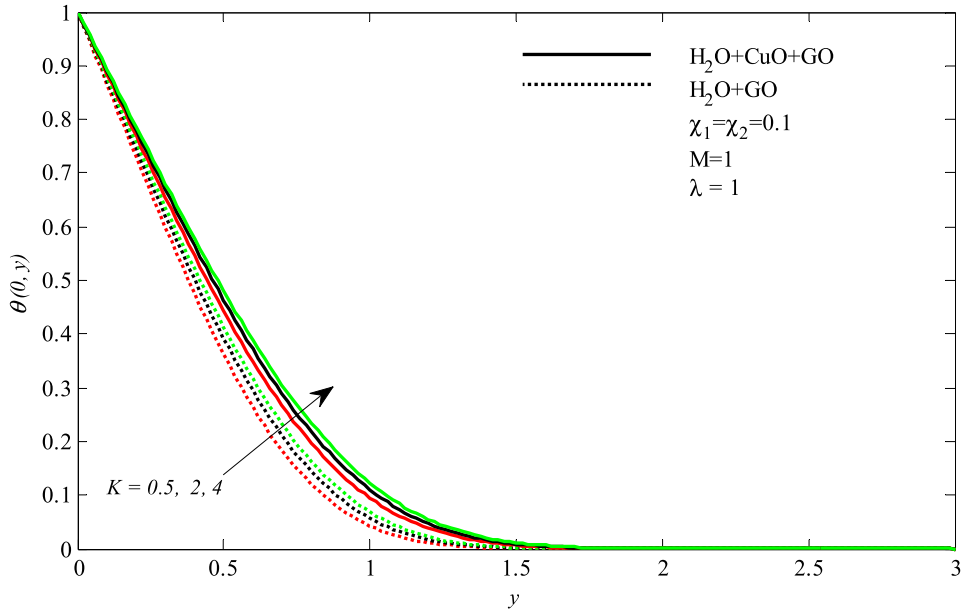

Fig. 11. Impact of micro rotation parameter K on the temperature profile.

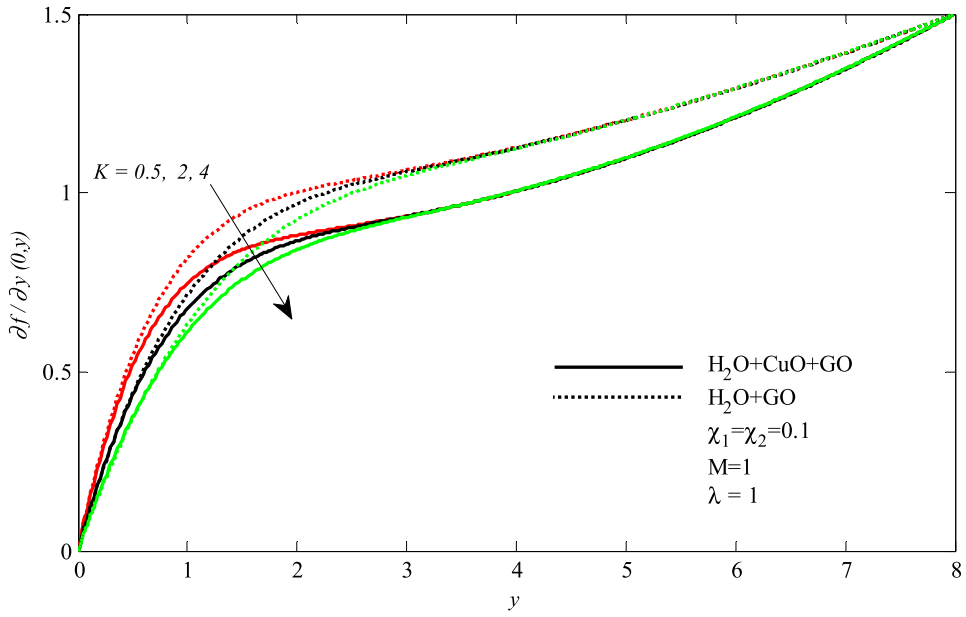

Fig. 12. Impact of micro rotation parameter K on the velocity profiles.

vertical distances from the sphere surface, the temperature is higher in the case of using hybrid instead of mono NF; also, the temperature is increased by increasing the micro-rotation parameter. The effect of altering K on the fluid temperature is not the same in all values of y, and it works only near the sphere surface in the thermal boundary layer region. At y = 0.6, by increasing the value of K from 0.5 to 4, the non-dimensional temperature increased from 0.18 to 0.22 and from 0.35 to 0.4 in cases of using mono and hybrid NF. The increasing effect of using hybrid NF and increasing K value on temperature.

The effect of employing different K values on velocity profile in cases of using mono and hybrid NFs is shown in Fig. 12. As seen, different values of micro rotation parameters show their effect in most vicinity of the sphere surface ($y < 3$). In this region, increasing K would supers the velocity, which could be attributed to the values of viscosity in K. In addition, at each y, the velocity is higher in the case of using mono NF. This is due to the higher viscosity of mono NF than hybrid NF, which would eventually give rise to boundary layer growth in this case. The variation of angular velocity vs different K values in cases of using mono and hybrid NF is depicted in Fig. 13. By comparing Fig. 12 and Fig. 13, a near similarity trend between the variations of velocity and angular velocity could be seen and, in each case, the angular velocity increases through the way from the sphere surface. The separation point and the resulting reverse flow are observed for K values of 2 and 4, which take place near the vicinity of the sphere surface. By getting away from the sphere surface to y = 0.5, the angular velocity changes from −0.14 to −0.195 and −0.175 for K value of 4 and in cases of using mono and hybrid NF, respectively. The higher reducing effect of mono NF than hybrid NF.

4.2.3. *The impact of mixed convection factor*

The mixed convection factor determines the type of heat convection and its direction; the higher the value of λ, the heat convection would be more natural and vice versa. The variation of temperature, velocity, and

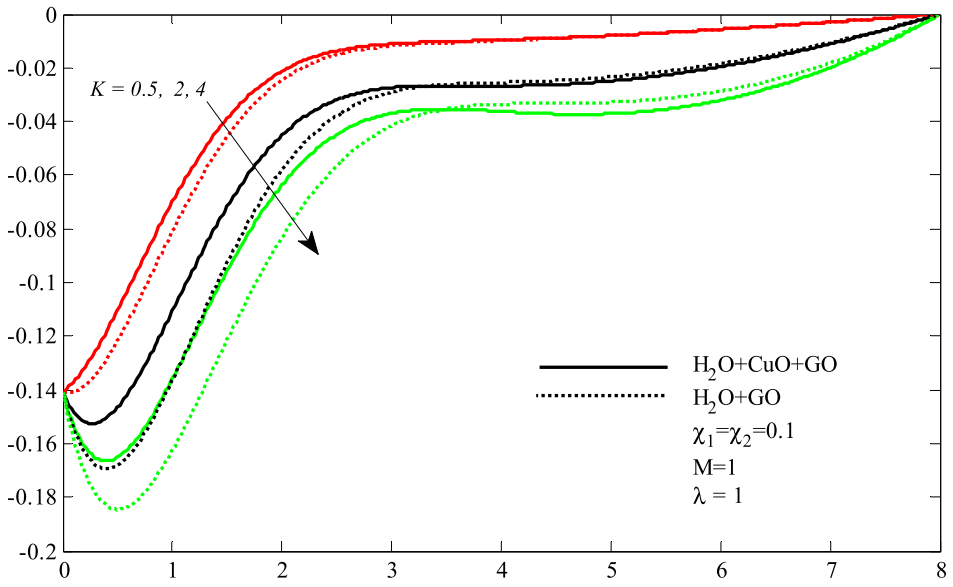

Fig. 13. Impact of micro rotation parameter K on the angular velocity profiles.

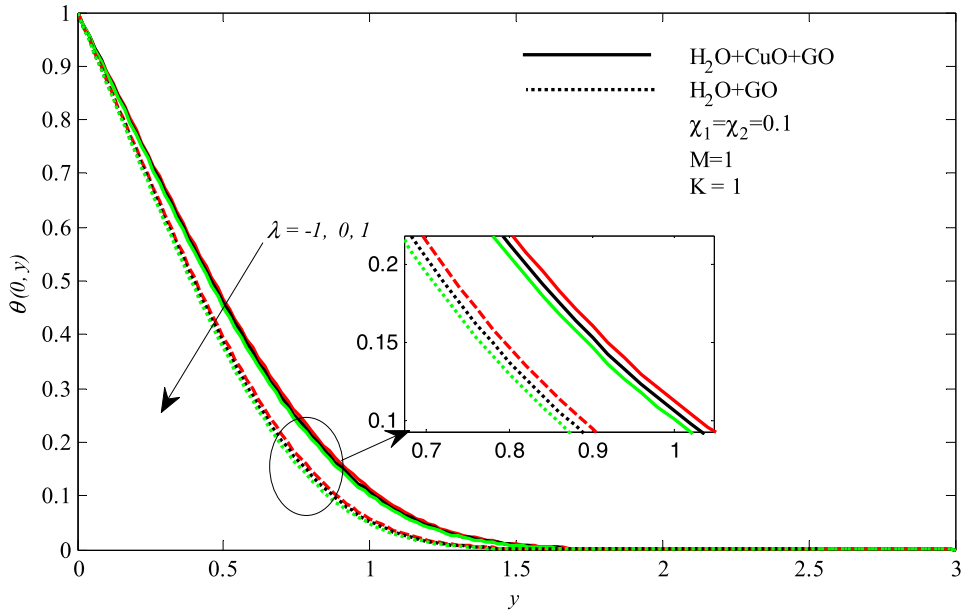

Fig. 14. Impact of mixed convection parameter λ on the temperature profiles.

angular velocity along the vertical distance from the sphere surface at the stagnation point ($x = 0$) for different mixed convection parameters is illustrated in Fig. 14, Fig. 15 and Fig. 16, respectively. As could be seen in Fig. 14, the temperature in the case of using hybrid NF is greater than mono NF, which could be attributed to higher thermal conductance. Furthermore, by raising the mixed convection factor from −1 to 0 and from 0 to 1, the temperature is increased; the temperature increase in the first section is due to converting the convection type from natural to force and in the second part, from the forced convection to heated type flow. The heated natural flow with its upward induced flow would enhance the fluid temperature.

Similar to the aforementioned temperature profile trends discussed in Fig. 14, the linear and angular velocities, as depicted in Fig. 15 and Fig. 16, increased by increasing y. it is worth noting that at each location, the linear velocity is the highest in the case of using mono NF, whereas, about the angular velocity, the highest value is for hybrid NF.

5. Conclusion

The numerical simulation of mixed convection boundary-layer flow around an isothermal solid sphere is presented in this study; two fluid types of hybrid and mono micropolar nanofluids with constant wall temperature in an MHD field are examined. The sensitivity analysis unveiled the influence of the mixed convection factors, the field strength and the micro-rotation factor. From this study, the following results were obtained:

- The improving effect of using NF by the induced micro-rotational effect is more prominent at lower angles and diminished at higher angles. Another point that could be obtained is that by increasing the magnetic parameter, the thermal boundary layer thickness is increased;
- By increasing the M value from 0.5 to 2, the thermal boundary layer thickness increased from 1.4 to 1.8. Also,

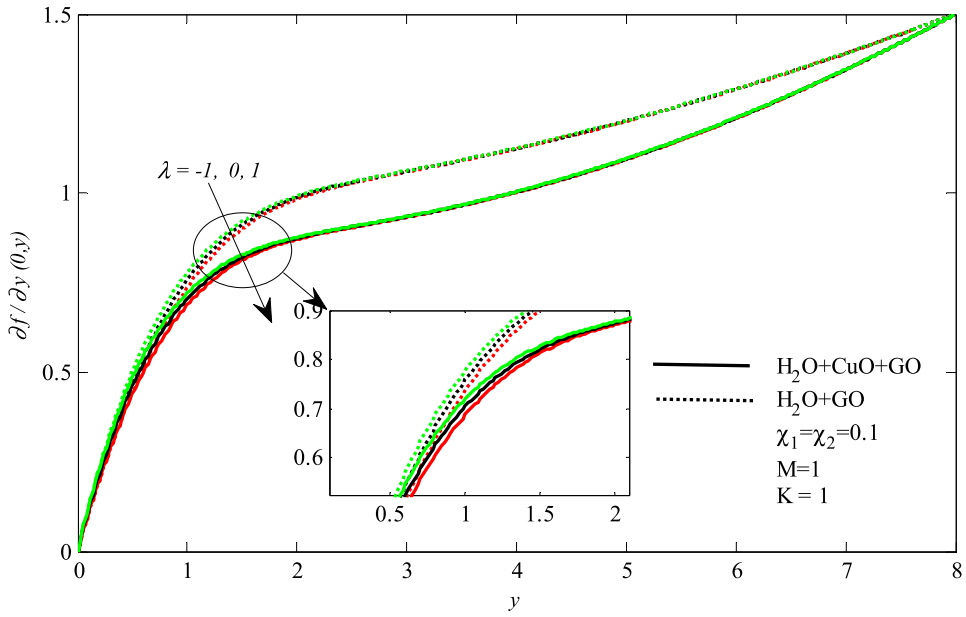

Fig. 15. Impact of mixed convection parameter λ on the velocity profiles.

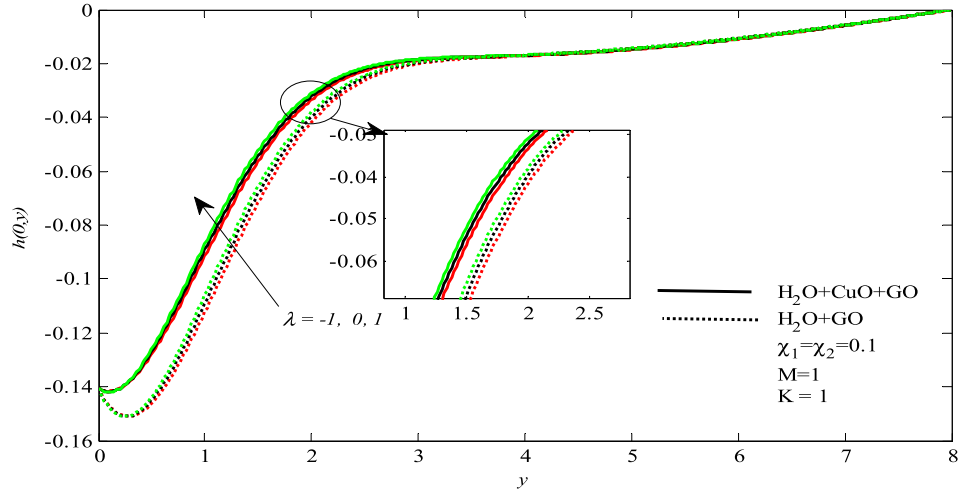

Fig. 16. Impact of mixed convection parameter λ on the angular velocity profiles.

- Using hybrid instead of mono NF has nearly no effect on altering the angular velocity at y values>4, and for other ones ($y < 4$), the difference is<15 %.
- The temperature is increased by increasing the micro-rotation parameter.
- The effect of altering K on the fluid temperature is not the same in all values of y, and it works only near the sphere surface in the thermal boundary layer region.

6. Author statement

- The corresponding author is responsible for ensuring that the descriptions are accurate and agreed by all authors.
- The role(s) of all authors are listed.
- Authors have contributed in multiple roles.

CRediT authorship contribution statement

Hamzeh T. Alkasasbeh: Methodology, Software, Validation, Writing – original draft. **Feras M Al Faqih:** Methodology, Software, Validation, Writing – original draft, Investigation. **As'ad Alizadeh:** Methodology, Software, Validation, Writing – original draft, Investigation. **Aissa abderrahmane:** Methodology, Software, Validation, Writing – original draft, Investigation. **Mohammad Ali Fazilati:** Methodology, Software, Validation, Writing – original draft, Investigation. **Hussein Zekri:** Methodology, Software, Validation, Writing – original draft, Investigation. **Davood Toghraie:** Methodology, Software, Validation, Writing – original draft, Investigation. **Abed Mourad:** Methodology, Software, Validation, Writing – original draft, Investigation. **Kamel Guedri:** Methodology, Software, Validation, Writing – original draft. **Obai Younis:** Methodology, Software, Validation, Writing – original draft, Investigation.

Declaration of Competing Interest

The authors declare that they have no known competing financial interests or personal relationships that could have appeared to influence the work reported in this paper.

Data availability

No data was used for the research described in the article.

Acknowledgements

The authors would like to thank the Deanship of Scientific Research at Umm Al-Qura University for supporting this work by Grant Code: (23UQU4331317DSR111).

References

[1] B. Keshtegar, J.A.F.O. Correia, N.-T. Trung, Optimisation of nanocomposite pipes under internal fluid reinforced by FRP and CNTs under seismic load, Int. J. Hydromechatronics 3 (3) (2020) 213–227.
[2] B. Keshtegar, M.L. Nehdi, Machine learning model for dynamical response of nano-composite pipe conveying fluid under seismic loading, Int. J. Hydromechatronics 3 (1) (2020) 38–50.
[3] Qu, M., Liang, T., Hou, J., Liu, Z., Yang, E.,... Liu, X. (2022). Laboratory study and field application of amphiphilic molybdenum disulfide nanosheets for enhanced oil recovery. Journal of Petroleum Science and Engineering, 208, 109695. doi: 10.1016/j.petrol.2021.109695.
[4] WANG. Xiaoming, LI. Changhe, ZHANG. Yanbin, SAID. Zafar, DEBNATH. Sujan, SHARMA. Shubham, YANG. Min, GAO. Teng, Influence of texture shape and arrangement on nanofluid minimum quantity lubrication turning, The International Journal of Advanced Manufacturing Technology 119 (1–2) (2022) 631–646, https://doi.org/10.1007/s00170-021-08235-4.
[5] X. Cui, C. Li, Y. Zhang, Z. Said, S. Debnath, S. Sharma, H.M. Ali, M. Yang, T. Gao, R. Li, Grindability of titanium alloy using cryogenic nanolubricant minimum quantity lubrication, Journal of Manufacturing Processes. 80 (2022) 273–286, https://doi.org/10.1016/j.jmapro.2022.06.003.
[6] DUAN. Zhenjing, LI. Changhe, ZHANG. Yanbin, YANG. Min, GAO. Teng, LIU. Xin, LI. Runze, SAID. Zafar, DEBNATH. Sujan, SHARMA. Shubham, Mechanical behavior and Semiempirical force model of aerospace aluminum alloy milling using nano biological lubricant, Front. Mech. Eng. (2022), https://doi.org/10.1007/s11465-022-0720-4.
[7] M. Shojaie, One-pot Multicomponent synthesis of pyrano[2,3-c]pyrazoles catalyzed by Copper oxide nanoparticles (CuO NPs), J. Synth. Chem. 1 (2022) 125–131, https://doi.org/10.22034/jsc.2022.155286.
[8] M.S. Shafik, CuI nanoparticles immobilized on magnetic nanoparticles catalyzed synthesis of diaryl ethers through C-O cross-coupling of phenols with aryl iodides, J. Synth. Chem. 1 (2022) 132–136, https://doi.org/10.22034/jsc.2022.155287.
[9] D. Domyati, CHARACTERIZATION OF BIOFABRICATION COPPER (II) OXIDE NANOPARTICLES AND INVESTIGATE THE PHOTOCATALYTIC EFFICIENCY, European Chemical Bulletin 11 (2) (2022) 1–6, https://doi.org/10.31838/ecb/2022.11.02.001.
[10] GAO. Teng, ZHANG. Yanbin, LI. Changhe, WANG. Yiqi, CHEN. Yun, AN. Qinglong, ZHANG. Song, LI. Hao Nan, CAO. Huajun, ALI. Hafiz Muhammad, ZHOU. Zongming, SHARMA. Shubham, Fiber-reinforced composites in milling and grinding: machining bottlenecks and advanced strategies. Frontiers of, Mechanical Engineering 17 (2) (2022) 24, https://doi.org/10.1007/s11465-022-0680-8.
[11] K.A.M. Alharbi, M.N. Alshahrani, N. Ullah, et al., Cattaneo-Christov heat flow model for copper–water nanofluid heat transfer under Marangoni convection and slip conditions, Sci Rep 12 (2022) 5360, https://doi.org/10.1038/s41598-022-09275-w.
[12] D.S. Toghraie, N. Sina, M. Mozafarifard, A. Aa, F. Soltani, M.A. Fazilati, Prediction of dynamic viscosity of a new non-Newtonian hybrid nanofluid using experimental and artificial neural network (ANN) methods, Heat Transfer Research. 51 (15) (2020).
[13] Y. Zheng, H. Yang, M.A. Fazilati, D. Toghraie, H. Rahimi, M. Afrand, Experimental investigation of heat and moisture transfer performance of CaCl2/H2O-SiO2 nanofluid in a gas–liquid microporous hollow fiber membrane contactor, International Communications in Heat and Mass Transfer. 113 (2020), 104533.
[14] D. Yılmaz Aydın, M. Gürü, Nanofluids: preparation, stability, properties, and thermal performance in terms of thermo-hydraulic, thermodynamics and thermo-economic analysis, Journal of Thermal Analysis and Calorimetry (2021).
[15] M.S. Kamel, F. Lezsovits, A.K. Hussein, Experimental studies of flow boiling heat transfer by using nanofluids, Journal of Thermal Analysis and Calorimetry 138 (6) (2019) 4019–4043.
[16] S.E. Ahmed, A.K. Hussein, H.A. Mohammed, S. Sivasankaran, Boundary layer flow and heat transfer due to permeable stretching tube in the presence of heat source/sink utilizing nanofluids, Applied Mathematics and Computation 238 (2014) 149–162.
[17] K. Ghachem, A.K. Hussein, L. Kolsi, O. Younis, CNT–water nanofluid magneto-convective heat transfer in a cubical cavity equipped with perforated partition, The European Physical Journal Plus 136 (4) (2021) 1–22.
[18] B. Ali, S. Hussain, Y. Nie, A.K. Hussein, D. Habib, Finite element investigation of Dufour and Soret impacts on MHD rotating flow of Oldroyd-B nanofluid over a stretching sheet with double diffusion Cattaneo Christov heat flux model, Powder Technology 377 (2021) 439–452.
[19] B. Ruhani et al., Statistical investigation for developing a new model for rheological behavior of Silica–ethylene glycol/Water hybrid Newtonian nanofluid using experimental data, Physica A: Statistical Mechanics and its Applications,. 525 (2019), 616-627.
[20] B Ruhani, et al., Statistical investigation for developing a new model for rheological behavior of ZnO–Ag (50%–50%)/Water hybrid Newtonian nanofluid using experimental data, Physica A: Statistical Mechanics and its Applications 525 (2019) 741–751.
[21] W. He, et al., Using of artificial neural networks (ANNs) to predict the thermal conductivity of zinc oxide–silver (50%–50%)/water hybrid Newtonian nanofluid, Int. Commun. Heat Mass Transf. 116 (2020) 104645.
[22] S. Salman, A.R.A. Talib, S. Saadon, M.T.H. Sultan, Hybrid nanofluid flow and heat transfer over backward and forward steps: A review, Powder Technology. 363 (2020) 448–472.
[23] A.S. Dalkılıç, Ö. Açıkgöz, B.O. Küçükyıldırım, A.A. Eker, B. Lüleci, C. Jumpholkul, et al., Experimental investigation on the viscosity characteristics of water based SiO2-graphite hybrid nanofluids, International Communications in Heat and Mass Transfer. 97 (2018) 30–38.
[24] A.K. Hussein, L. Kolsi, M.A. Almeshaal, D. Li, H.M. Ali, I.S. Ahmed, Mixed convection in a cubical cavity with active lateral walls and filled with hybrid graphene–platinum nanofluid, Journal of Thermal Science and Engineering Applications 11 (4) (2019).
[25] P.M. Patil, S.H. Doddagoudar, H.F. Shankar, Influence of nonlinear thermal radiation on mixed convective hybrid nanofluid flow about a rotating sphere, Heat Transfer 51 (6) (2022) 5874–5895.
[26] M.M. Bhatti, O. Anwar Bég, R. Ellahi, M.H. Doranehgard, F. Rabiei, Electro-magnetohydrodynamics hybrid nanofluid flow with gold and magnesium oxide nanoparticles through vertical parallel plates, J. Magn. Magn. Mater. 564 (2022), 170136, https://doi.org/10.1016/j.jmmm.2022.170136.
[27] Alkasasbeh, H. (2022). Mathematical modeling of MHD flow of hybrid micropolar ferrofluids about a solid sphere. *Frontiers in Heat and Mass Transfer (FHMT), 18*.
[28] A.C. Eringen, Theory of micropolar fluids, Journal of Mathematics and Mechanics. (1966) 1–18.
[29] T. Ariman, M. Turk, N. Sylvester, Applications of microcontinuum fluid mechanics, International Journal of Engineering Science. 12 (4) (1974) 273–293.
[30] G. Lukaszewicz, Micropolar fluids: theory and applications, Springer Science & Business Media, 1999.
[31] O. Aydın, I. Pop, Natural convection in a differentially heated enclosure filled with a micropolar fluid, International Journal of Thermal Sciences. 46 (10) (2007) 963–969.
[32] N.S. Gibanov, M.A. Sheremet, H.F. Oztop, K. Al-Salem, MHD natural convection and entropy generation in an open cavity having different horizontal porous blocks saturated with a ferrofluid, J. Magn. Magn. Mater. 452 (2018) 193–204, https://doi.org/10.1016/j.jmmm.2017.12.075.
[33] M. Saleem, S. Asghar, M.A. Hossain, Natural convection flow of micropolar fluid in a rectangular cavity heated from below with cold sidewalls, Mathematical and Computer Modelling. 54 (1–2) (2011) 508–518.
[34] H. Hashemi, Z. Namazian, S. Mehryan, Cu-water micropolar nanofluid natural convection within a porous enclosure with heat generation, Journal of Molecular Liquids. 236 (2017) 48–60.
[35] A. Hussanan, M.Z. Salleh, I. Khan, S. Shafie, Convection heat transfer in micropolar nanofluids with oxide nanoparticles in water, kerosene and engine oil, Journal of Molecular Liquids. 229 (2017) 482–488.
[36] M. Izadi, S. Mehryan, M.A. Sheremet, Natural convection of CuO-water micropolar nanofluids inside a porous enclosure using local thermal non-equilibrium condition, Journal of the Taiwan Institute of Chemical Engineers. 88 (2018) 89–103.
[37] A. Abidi, Z. Raizah, J. Madiouli, Magnetic field effect on the double diffusive natural convection in three-dimensional cavity filled with micropolar nanofluid, Applied Sciences. 8 (12) (2018) 2342.
[38] H. Alfvén, Existence of electromagnetic-hydrodynamic waves, Nature. 150 (3805) (1942) 405–406.
[39] A. Rahbari, M. Abbasi, I. Rahimipetroudi, B. Sundén, D. Domiri Ganji, M. Gholami, Heat transfer and MHD flow of non-newtonian Maxwell fluid through a parallel plate channel: analytical and numerical solution, Mechanical Sciences. 9 (1) (2018) 61–70.
[40] S. Atif, S. Hussain, M. Sagheer, Effect of thermal radiation and variable thermal conductivity on magnetohydrodynamics squeezed flow of Carreau fluid over a sensor surface, Journal of Nanofluids. 8 (4) (2019) 806–816.
[41] R. Nazar, N. Amin, I. Pop, Mixed convection boundary layer flow about an isothermal sphere in a micropolar fluid, International journal of thermal sciences. 42 (3) (2003) 283–293.
[42] T. Cebeci, P. Bradshaw, Physical and computational aspects of convective heat transfer, Springer Science & Business Media, 2012.
[43] MEDEBBER, Mohamed A., AISSA, Abderrahmane, SLIMANI, Mohamed El Amine, et al. Numerical study of natural convection in vertical cylindrical annular enclosure filled with Cu-water nanofluid under magnetic fields. In : Defect and Diffusion Forum. Trans Tech Publications Ltd, 2019. p. 123-137.
[44] ABDERRAHMANE, AISSA, HATAMI, Mohammad, MEDEBBER, M. A., et al. Non-Newtonian nanofluid natural convective heat transfer in an inclined Half-annulus porous enclosure using FEM. Alexandria Engineering Journal, 2022, vol. 61, no 7, p. 5441-5453.
[45] RADOUANE, Fares, ABDERRAHMANE, Aissa, MEBAREK-OUDINA, Fateh, et al. Magneto-free convectiveof hybrid nanofluid inside non-darcy porous enclosure containing an adiabatic rotating cylinder. Energy Sources, Part A: Recovery, Utilization, and Environmental Effects, 2020, p. 1-16.